



An investigation of the relationship between position within coater and pyrolytic carbon characteristics using nanoindentation

Greg Hofmann^{a,*}, Martin Wiedenmeier^a, Matt Freund^a, Al Beavan^a, Jennifer Hay^b, G.M. Pharr^c

^a*Sulzer Carbomedics, Austin, TX, 78752 USA*

^b*NANO[®] Instruments, Oak Ridge, TN, 37830 USA*

^c*Department of Materials Science and Engineering, The University of Tennessee, Knoxville, TN, 37996, USA*

Received 24 January 1999; accepted 28 May 1999

Abstract

Pyrolytic carbon samples were formed at several locations within a fluidized bed reactor by depositing onto stationary graphite rods, which were suspended parallel to the coater's axis. The samples were examined metallographically and using nanoindentation. The sample densities and mass deposition rate as a function of position were also determined. Homogeneous material was formed primarily at positions along the coater's central axis and near the reactor's gas inlet. Porous coatings were formed far from the central axis or far from the gas inlet. Nanoindentation measurements indicated the homogeneous material had a higher elastic modulus and hardness and greater elastic recovery, as compared to the porous material. Both materials were seen to be isotropic. The homogeneous coatings were seen to be the densest and the mass deposition rate was seen to increase with increasing distance from the gas inlet. It has been proposed that these observations can be explained in light of the spatial distribution of the time averaged fluidized bed particle kinetic energy and number density. © 2000 Elsevier Science Ltd. All rights reserved.

Keywords: A. Pyrolytic carbon; C. Optical microscopy, SEM; D. Elastic properties, Porosity

1. Introduction

Prosthetic heart valves are fabricated routinely from pyrolytic carbon (PyC) using a fluidized bed reactor [1,2]. The heart valve components are fabricated by depositing PyC onto graphite mandrels or substrates, and machining the coated parts to desired specifications.

The fluidized bed employed in the work described here exhibits a spouting behavior, as has been described previously [3]. The expected differences in the average bed particle energy and number density between the central spout region and the annulus region provide motivation for exploring deposition behavior at the coater's center and near the coater's wall. In an effort to investigate the

relationship between these positions and PyC characteristics, samples of PyC were fabricated at locations near the coater's central axis and near the coater's wall. The samples were examined metallographically, elastic modulus and hardness measurements were made using a nanoindenter, and densities were determined using a sink-float method.

The metallographic analysis revealed the presence of two different types of material, the first being smooth and homogeneous and the other having a rough and porous appearance. Both types were observed to be optically isotropic. The homogeneous material was formed predominantly at positions along the fluidized bed coater's central axis (Z-axis) and nearer to the reactor's gas inlet. The porous and rough material was found mostly at positions away from the coater's central axis and at positions further downstream from the gas inlet. The nanoindentation results indicate that the homogeneous material has higher elastic modulus and hardness and greater elastic recovery, as

*Corresponding author.

E-mail address: ghofmann@visus.jnj.com (G. Hofmann).

¹Present address: 1655 The Greensway, App 3324, Jacksonville Beach, Florida 32250, USA.

compared to the rough material. The PyC samples fabricated near the gas inlet were observed to have a higher density than those produced at positions further downstream.

The nanoindentation and density results are consistent with the notion that the homogeneous material is less porous than the rough material. In this work, the relationships among position within the reactor, the formation of either the homogeneous or the rough material, the expected fluidized bed particle kinetic energy and number density, and the proposed role of bed particle collisions are discussed.

2. Experimental

The fluidized bed reactor, used to produce PyC samples for the work presented here, has been described previously [1,2]. For each of several separate coating runs, graphite rods, (Poco® AXF-5Q) with a diameter of ~0.25 cm were suspended parallel to the coater axis at two radial positions. The first radial position (R1) was at the coater center, and the second (R2) was ~3 cm from the coater center. Since the diameter of the coater was about 7.6 cm, the rods coated at R2 were very near the coater wall.

The rods placed at R1 were suspended so that the rod end was about 5.0 to 7.5 cm from the position at which the gases first entered the conical shaped reactor tube. For reference purposes, the portion of the rod nearest the gas inlet during the coating run will be referred to as the 'upstream' portion of the rod; the opposite end is designated the 'downstream' end. Also, the position just above the point at which the gas first enters the conical portion of the reactor tube (gas inlet) is designated $Z=0.0$ cm. The rods at R2 were suspended so that the rod end was about 0.6 cm above the conical section of the reactor. This position corresponds to about $Z=13.3$ cm. For all runs, the rods were ~15.25 cm in length.

Six coating runs were executed, three runs with rods at R1 and three with rods at R2. The rods were coated using the process described in Ref. [1]. In each case, 6 l/min (STP) of propane and 12 l/min (STP) of nitrogen were employed as the coating gases. These gases were mixed prior to entering the reactor chamber. The operating temperature was 1350°C. This temperature was measured at the coater's wall. The coating bed was comprised of 500–700 micron ZrO_2 particles, with an initial charge of 200 g. During the run, 300–400 micron ZrO_2 particles were removed and added as described in Ref. [2]. Run times varied between 140 and 200 min. A summary of the runs is presented in Table 1. The second and third runs for the case where the rod was located at R2 were carried out using identical conditions in order to provide a rough estimate of the reproducibility of the experimental technique.

Following coating, the rods were marked at 1.25 cm

Table 1

Summary of coating times and positions of graphite rod substrates

Run ID	Run time (min)	Z-position of rod bottom (cm)	Radial position (cm)
R1(run1)	180	5.0	0.0
R1(run2)	160	7.5	0.0
R1(run3)	140	7.5	0.0
R2(run1)	200	13.3	3.0
R2(run2)	180	13.3	3.0
R3(run3)	180	13.3	3.0

intervals and cut, using a diamond saw, so as to expose a cross section of the coating corresponding to a specific radial and Z-position within the coater. Samples near these positions were also retained for density measurements.

The sectioned samples were mounted and polished using three different polishing pastes; in succession, those containing 9, 3, and 1 micron diamond particles were employed. The samples were analyzed visually with a Nikon Epiphot microscope using bright field and polarized light.

Additionally, elastic modulus and hardness measurements were made with the metallographic samples. Most elastic modulus and hardness measurements were made with a NANO Indenter® II, at the Oak Ridge National Laboratory, using a loading rate of 1500 $\mu N/s$ and a peak load of 30 mN. The system was calibrated using a fused silica sample. The elastic modulus and hardness of this sample were found to be within less than 5% of known values [4]. The calibration method and the method used to analyze the indentation load–displacement data are described elsewhere [5]. The modulus and hardness measurements made on the sample generated during R1(run1) were performed at NANO® Instruments Inc., using the Continuous Stiffness™ method [5].

When testing the samples generated at R1, care was taken to make indentations strictly in regions of homogeneous material. In some cases, these regions were seen to be narrow bands, with widths smaller than 100 μm , thus warranting the use of the nanoindenter. Indentations made on the R2 samples were made primarily in regions of rough material, which were typical for that sample. In one case, however, indentations were made on an R1 sample in a region of rough material and on an R2 sample in a region of homogeneous material. In all cases, at least five indentations were made on each sample.

Samples retained for density measurements were grit blasted with sodium bicarbonate in order to remove the graphite substrate and then broken into small pieces. Using a mixture of acetone and bromoform, a 10-ml Lurex® pycnometer, and a Mettler-Toledo AB104 balance, the sink-float method was employed to determine the density of the PyC specimens.

Some of the sectioned samples had a cross section with a near circular shape; other samples had a cross section

that was almost elliptical. As such, mass deposition rates were approximated according to

$$dm/dt = \rho(r - R_{\text{rod}})/t, \text{ (circular cross section)}$$

$$dm/dt = \rho[(a - R_{\text{rod}})b + (b - R_{\text{rod}})a]/(2 \times \sqrt{(a^2 + b^2)}/\sqrt{2})/t \text{ (elliptical cross section)}$$

where m is the mass, ρ is the density, R_{rod} is the initial radius of the rod, and t is the deposition time. In the former case, r is the radius of the circular shaped sample. In the latter case, $2 \times a$ is the minimum diameter of the elliptical cross section and $2 \times b$ is the maximum diameter.

3. Results

The PyC samples fabricated at R1 were smooth and had a dark gray appearance extending from the upstream point of the sample to about 7.5 to 10.0 cm toward the downstream end. The upstream tip of the rod was gray-silver in appearance and was more polished than any other portion of the sample. Near the downstream end of the rod, a black and sooty coating was formed. In general, the shape of the samples coated at R1 mimicked the shape of the rods; so, when the samples were cut into segments, the resultant sample cross-sections were approximately circular.

The upstream tip of the samples produced at R2 had an appearance similar to the tip of the R1 samples with a slightly less polished appearance. In this region, the cross section was nearly circular. In contrast, for positions greater than about 1.25 cm from the upstream tip, the shape of the samples produced at R2 did not duplicate the shape of the rod. Rather, when the R2 samples were sliced into portions, the cross-section was approximately elliptical. The elliptical shape was not centered about the axis of the rod, but was skewed toward the side of the sample that was nearest the reactor wall during the coating process. From about 1.25 cm to 5.0 cm from the upstream tip, the surface of the sample that was nearest the reactor wall was dark gray and smooth. The corresponding surface farthest from the wall was darker and less smooth, but it was not sooty. A black and sooty coating was seen to extend from about 5.0 cm from the upstream tip to the downstream end of the sample.

The position at which the coating surface changed from dark gray and smooth to a sooty appearance was between $Z=15.0$ cm and 18.0 cm for both the R1 and R2 samples.

Metallographic analysis of the samples generally distinguished two types of material: one that was smooth and homogeneous and another that was rough and porous. In both cases, no distinct grains could be observed under bright field or polarized light conditions. Additionally, when viewed under polarized light conditions, such that

the reflected light from the surface was at a minimum, no Maltese Cross pattern could be observed [6].

Samples produced at R1 with Z -positions less than about 10.0 cm were comprised almost entirely of the homogeneous material. An example of such a sample is presented in Fig. 1. At magnifications of $400\times$, this homogeneous material exhibits only a small degree of porosity. Samples produced at Z -positions of about 10.0 cm had a number of regions of the rough material that were contained within bands. The bands were observed to be concentric with the rod axis; however, in some cases, the bands were seen to be interrupted. The size and frequency of the bands increased with increasing Z -position, such that at Z -positions greater than 15.0 cm, most of the sample was composed of the rough material, although some concentric bands of the homogeneous material were observed. An example of a sample with a small amount of the rough material is given in Fig. 2 and a representative image of a sample comprised mostly of the rough material is presented in Fig. 3. At magnifications of $400\times$, the rough material is observed to be quite porous.

Coatings formed at R2 near the upstream tip were composed mostly of the homogeneous material. Above about 1.25 cm from the upstream tip, the coatings produced at R2 were either composed of the homogeneous material or the rough material; coatings deposited on the rod surface that was closest to the wall were comprised of the homogeneous material; coatings formed on the rod surface that was farthest from the wall were composed of the rough material. An example of this is given in Fig. 4. Regardless of whether the coatings were produced at R1 or R2, very rough and dark coatings were fabricated at Z -positions greater than 15.0 cm.

Plots of load and displacement, representative of the

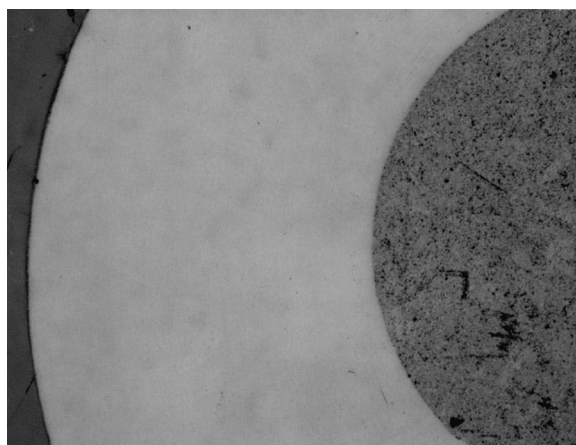


Fig. 1. An example of PyC found in a homogeneous material region. This sample was produced during R1(run1) at a position of about $Z=7.5$ cm. The graphite rod is seen near the right side of this image.

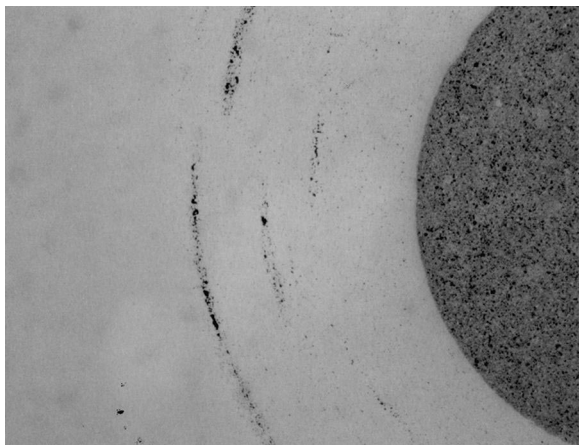


Fig. 2. An example of a sample having bands of the rough and more porous material embedded in the homogeneous material. This sample was produced during R1(run3) at a position of about $Z=13.0$ cm.

nanoindentation data obtained for the homogeneous and rough materials, are presented in Fig. 5. The corresponding modulus and hardness results are presented in Figs. 6 and 7. The modulus data for the homogeneous PyC are distributed about 24.4 ± 0.8 GPa, and the modulus of the rough material is spread about 8.8 ± 1.9 GPa. The hardness of the homogeneous PyC is scattered about 3.6 ± 0.2 GPa; the hardness of the rough PyC is distributed about 0.9 ± 0.2 GPa. In all cases, the error was set to the pooled standard deviation of each data set associated with the indentations made in a given region.

Lastly, the densities, which are seen to decrease with increasing position from the gas inlet, and mass deposition rates, which are seen to increase with increasing position from the gas inlet, are plotted in Figs. 8 and 9.

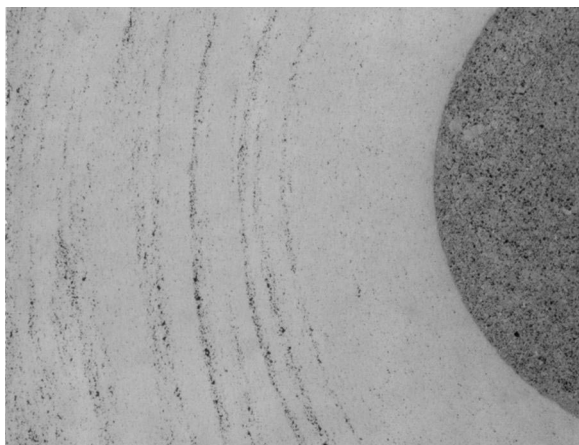


Fig. 3. An example of rough and porous PyC. This sample was produced during R1(run3) at a position of about $Z=16.5$ cm.

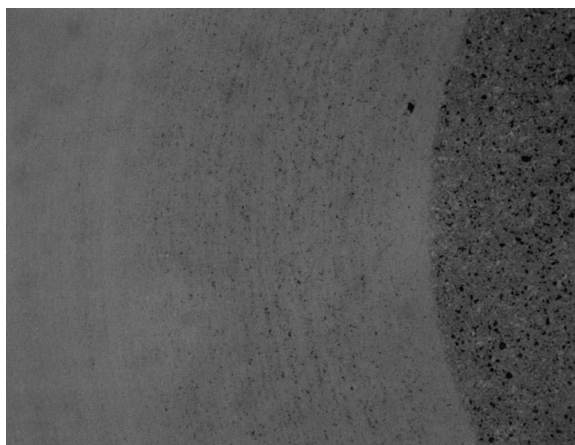


Fig. 4. An example of the rough and porous PyC coating formed near the coater wall. This sample was formed during R2(run2) at a position of about 18.5 cm.

4. Discussion

As mentioned in Section 2, the second and third runs for the case where the rod was located at R2 were carried out using identical conditions in order to provide a rough estimate of the reproducibility of the experimental technique. Examination of Fig. 8 indicates that most of the scatter in the data occur for Z -positions between about 13 and 15 cm (positions near the time averaged maximum height of the bed). The data in Fig. 9 show that the mass deposition rates for these samples agree well over most positions. Additionally, the second and third runs for the case where the rod was located at R1 show good agreement between the densities, from the two runs, of samples produced at positions below about 13 cm (Fig. 8) and mass deposition rates below about 16 cm (Fig. 9). Only the run times were different in these experiments. These results suggest that the experimental technique is capable of reproducing samples at positions where it is likely that the substrate was contained in the bed.

The metallographic analysis revealed the presence of two types of material whose formation appears to depend upon position within the coater. The homogeneous material was found mostly in the spout region nearer to the gas inlet and the rough material was formed within the annulus region and at positions far from the gas inlet. The lack of distinct grains and a 'cross' pattern indicates that both the homogeneous and rough materials can be described as optically isotropic, as defined in Ref. [1]. The metallographic analysis shows that the rough material is more porous than the homogeneous material.

The load and displacement curves associated with the modulus and hardness determinations show that homogeneous PyC is more elastic than the rough material. Regardless of where the material was formed, results

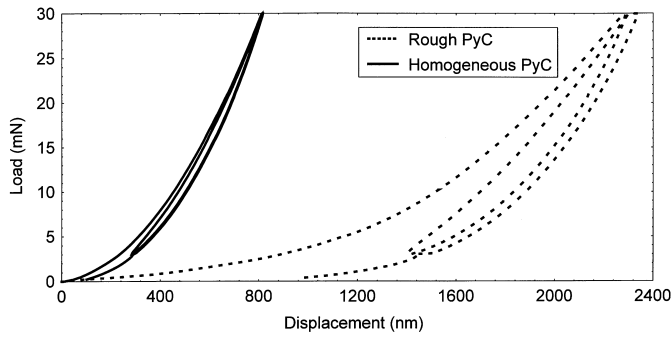


Fig. 5. Load–displacement curves generated using the nanoindenter. For both load–displacement traces, the top portion of the curve represents the loading sequence and the unloading data are traced in the bottom portion of the curve. The unloading portion of the curve for the homogeneous material is seen to return almost to the point where the loading curve was initiated; this is in contrast to that for the rough material. This indicates that the homogeneous material has nearly full elastic recovery and the rougher and more porous material has greater plasticity.

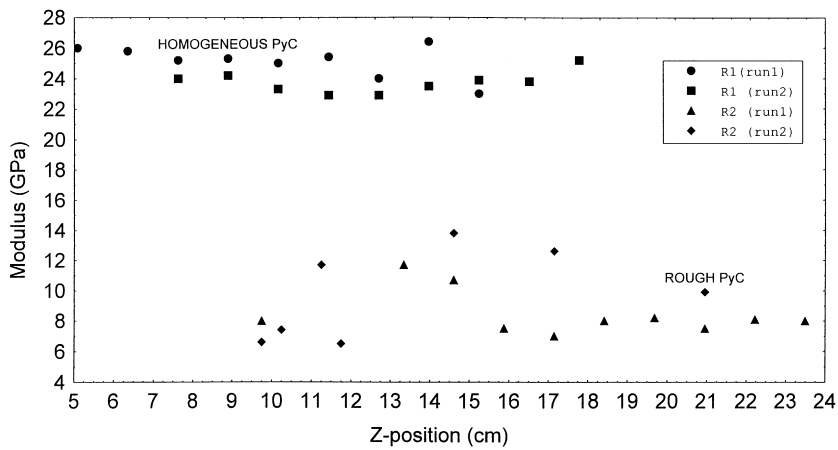


Fig. 6. The elastic modulus of samples fabricated at various Z-positions and at two radial positions. These measurements indicate that the homogeneous material has a higher elastic modulus.

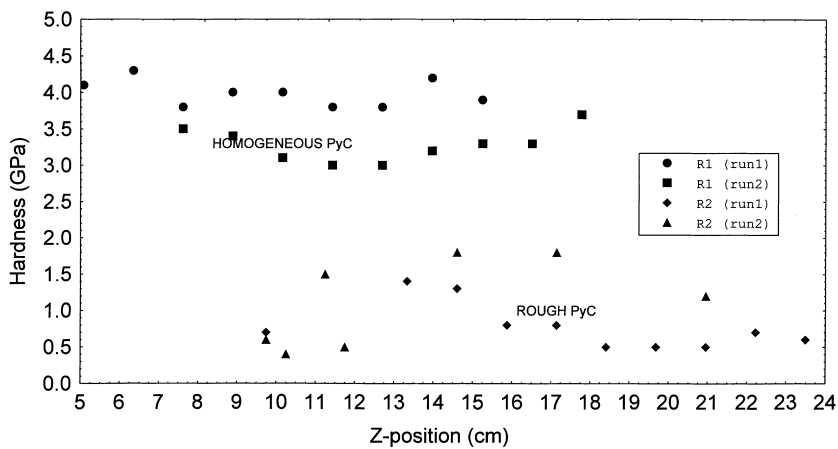


Fig. 7. The hardness of samples fabricated at various Z-positions and at two radial positions. These measurements indicate that the homogeneous material has a higher hardness.

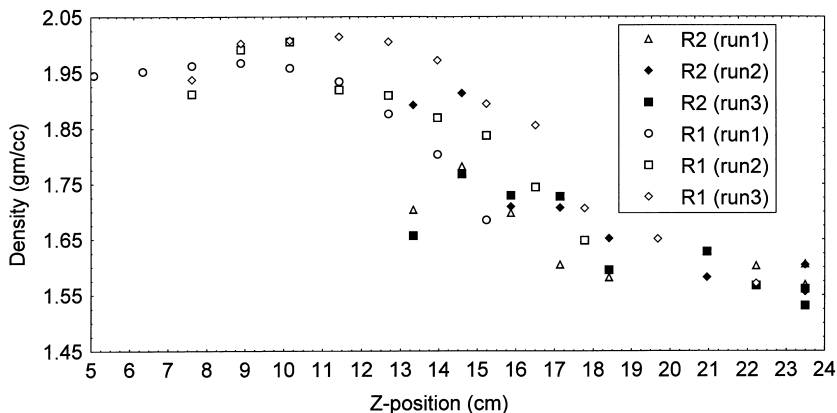


Fig. 8. Densities of samples fabricated at various Z-positions and at two radial positions. These measurements indicate that the densest samples are those produced at lower Z-positions. R2, radial position near wall; R1, central axis.

indicate that the homogeneous material had a higher modulus and hardness than the rough material. The density determinations reveal that at higher Z-positions, where the presence of the rough material is observed to be greatest, the coating density is lowest. The least porous coatings (homogeneous material) are formed along the coater's central axis and within 5.0 and 10.0 cm from the point at which the gas first enters the reactor. More porous coatings are produced at positions far from the coater's central axis and at positions along the central axis, but 10.0 to 15.0 cm from the gas inlet. Very rough, porous, and sooty coatings are produced at positions greater than 15.0 cm from the gas inlet, regardless of the radial location.

The fluidized bed used in the experiments described here has been characterized as having a central region where the bed particles are fluidized in a spouting manner and an

area surrounding the spout referred to as the annulus region [3]. The spouting region is characterized, generally, as having more energetic bed particles and a smaller number density of bed particles as compared to that in the annulus region. Additionally, for the conditions described in Section 2, the time averaged bed height would not exceed $Z=15.0$ cm, except for momentary and large spouts of bed material.

The data in Fig. 9 indicate that the mass deposition rate is lowest near the gas inlet and highest at positions far from the gas inlet, where the time averaged bed particle density is expected to be very low. Far from the gas inlet the surface area available to the depositing carbon species, per unit volume (S/V), is small, as compared to lower Z-position regions. This lower S/V ratio may lead to the formation of the sooty coatings found at positions far from

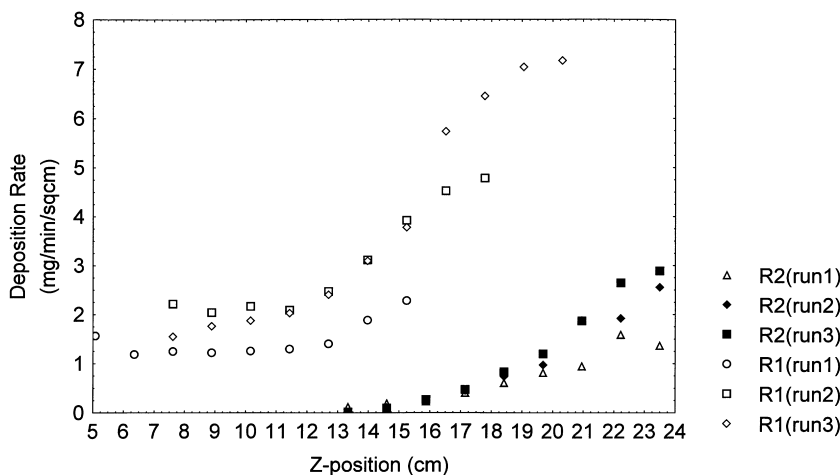


Fig. 9. Mass deposition rates corresponding to samples fabricated at various Z-positions and at two radial positions. Measurements show deposition rates are highest in regions where source gas density is relatively high and where bed particle kinetic energy is relatively low.

the gas inlet. However, the S/V ratio is also expected to be low near the gas inlet, as opposed to positions nearer to the wall, due to smaller number of bed particles in the spout. As such, it seems that a change in the S/V ratio cannot account solely for the difference in the mass deposition rates. Furthermore, one might expect the rate to be higher at positions near the gas inlet since the source gas density near the inlet is expected to be higher, as compared to the annulus region, or regions far from the gas inlet.

With these points in mind, it is suggested that the bed particles' kinetic energy may influence whether the homogeneous or porous coatings are formed. Specifically, it is suggested that the bed particles act to polish the growing coating, and this is reflected in the higher mass deposition rate where less polishing occurs. Thus, for the conditions used in the work described here, when depositing in regions where the bed particle kinetic energy is low, porous coatings are formed and in regions where the energy is high, (and everything else is nearly equivalent) denser and more homogeneous coatings are formed. For regions where the bed particle number density approaches zero, very porous and sooty coatings are formed.

To test this hypothesis, several experiments have been executed and they are described briefly as follows. In separate experiments, different types of substrates (stationary rods and free floating rectangular slabs) were coated using conditions similar to that described above. Prior to coating, V-shaped notches were cut into these substrates. In all cases, the width of a notch at its opening was about 350 microns, so that during the coating process, bed particle collisions within the notch were reduced or eliminated. After coating, each sample was investigated using SEM with attention paid to the coating deposited within and just outside of the notch sites. In some cases, the coated samples were fractured at the notch sites and examined. An example of such a sample is presented in Fig. 10. For this case, a stationary rod with a notch cut into the rod perimeter was suspended along the coater's central axis and coated using conditions similar to that for runs R1(run2) and R1(run3). Only the run time was different. When positioned along the coater's central axis, the notch on the rod was at about $Z=10.0$ cm so bed particle collisions with the coating deposited just outside of the notch likely occurred. After coating, the rod was fractured at the notch site and examined using SEM. Examination of the image presented in Fig. 10 shows that the coating deposited within the notch is quite porous and the coating deposited outside of the notch has a much denser appearance. These results are consistent with the notion that bed particle collisions with the growing coating are important for forming a dense and homogeneous coating.

Evidence that bed particle collisions are important to forming dense PyC has been found previously in a study of coatings deposited in a tumbling bed [7]. In this work, it was observed that coatings deposited at higher tumbling bed rotational speeds were more compact and less porous

than those deposited at lower bed rotational speeds. The coatings deposited at the higher bed rotational speeds were also found to be denser, while the PyC coating crystallite size and preferred orientation were seen to be independent of the bed rotational speed. It is expected that higher rotational tumbling bed speeds should translate to more energetic and more frequent collisions between the bed particles and the depositing coating.

Lastly, numerical models of a fluidized bed reactor should be able to predict the time averaged bed particle kinetic energy and density as a function of position. Further support for this hypothesis could be gained if the models showed a higher bed particle energy density at positions where the homogeneous material was experimentally produced. Presently, attempts at correlating these experimental results with those from a numerical model of this reactor are underway [8].

5. Summary

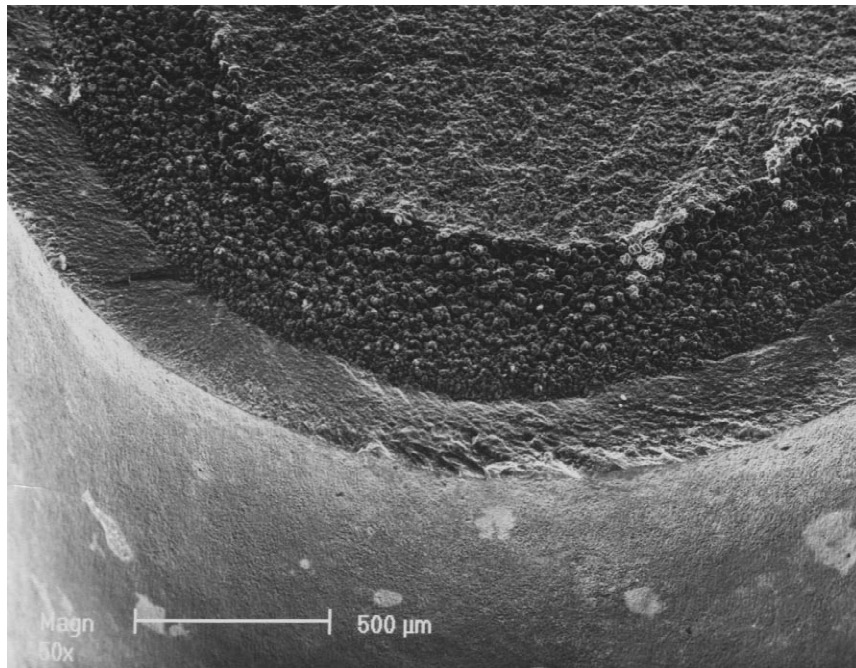
In an effort to explore the relationship between the position within a fluidized bed reactor and several PyC characteristics, samples of PyC were fabricated at specific positions within the reactor and subsequently analyzed. The samples were examined metallographically, elastic modulus and hardness measurements were made using a nanoindenter, and densities were determined using a sink-float method.

The metallographic analysis indicated that two types of isotropic PyC could be distinguished: a homogeneous material and a rough material. The type of material formed depends on the position within the fluidized bed reactor at which the coatings were deposited. Metallographic examinations and density measurements indicate that the homogeneous material is less porous than the rough material. Nanoindentation shows that the homogeneous material is more elastic and has a higher elastic modulus and hardness as compared to the rough material.

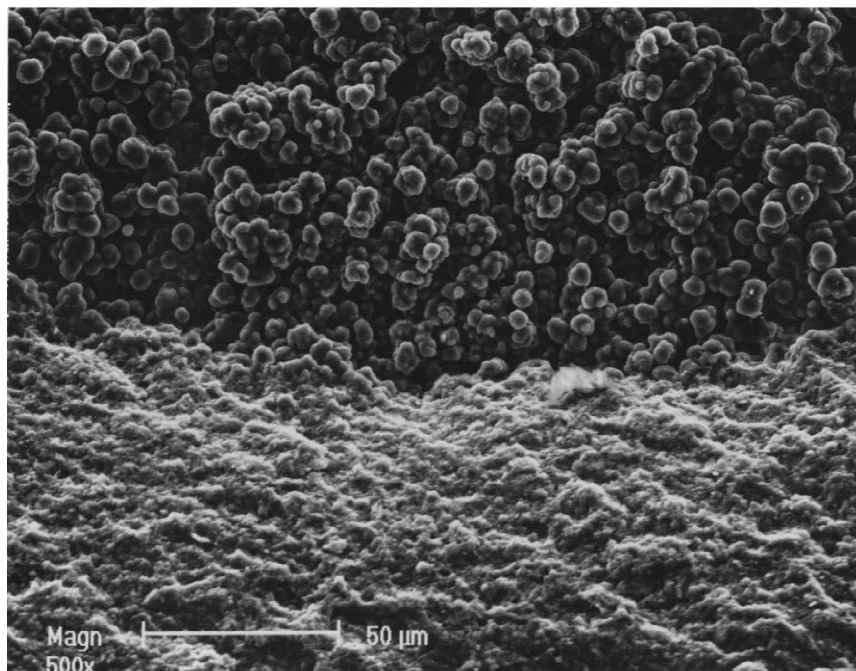
It is proposed that whether the homogeneous or rough material is formed is related to the bed particle kinetic energy.

Acknowledgements

The authors acknowledge the contributions of Cephas Wozencraft, Randy Weldy, and Richard Mangrum in preparing the samples, performing density measurements, and in obtaining micrographs. Jim Byrant was responsible for the SEM images. The authors thank Jack Hay for deriving the nanoindenter shape function. This research was sponsored in part by the Division of Materials Sciences, US Department of Energy, under the contract DE-AC-96OR22464 with Lockheed Martin Energy Research Corp., and through the SHaRE Program under



(a)



(b)

Fig. 10. SEM images of a coating cross section showing the coating deposited within and outside of the notch. At the top of the lower magnification image, the graphite core can be seen. Just below this, the coating deposited within the notch, which was not exposed to bed particle collisions, is seen. Below this, the coating deposited outside of the notch is shown. The higher magnification image shows the interface between the coating formed in the absence of bed particle collisions and the coating exposed to bed particle collisions. It is seen that the coating exposed to bed particle collisions is more dense than that formed in regions where bed particle collisions were restricted or eliminated. This coating was produced along the coater's central axis at about $Z=10$ cm.

contract DE-AC05-76OR0033 between the US Department of Energy and Oak Ridge Associated Universities.

References

- [1] Bokros JC. The structure of pyrolytic carbon deposited in a fluidized bed. *Carbon* 1965;3(1):17–29.
- [2] Akins RJ, Bokros JC. The deposition of pure and alloyed isotropic carbons in steady-state fluidized beds. *Carbon* 1974;12(3):439–52.
- [3] Guilleray J, Lefevre RLR, Price MST. Pyrocarbon coatings of nuclear fuel particles. In: Walker Jr. PL, Thrower PA, editors, *Chemistry and physics of carbon*, Vol. 15, New York: Dekker, 1979, pp. 1–108.
- [4] Simmons G, Wang H eds. *Single crystal elastic constants and calculated aggregate properties: a handbook*, 2nd ed, Cambridge MA: MIT Press, 1971.
- [5] Oliver WC, Pharr GM. An improved technique for determining hardness and elastic modulus using load and displacement sensing indentation experiments. *J Mater Res* 1992;7(6):1546–83.
- [6] Gray RJ, Cathcart JV. Polarized light microscopy of pyrolytic carbon deposits. *J Nucl Mater* 1966;19:81–9.
- [7] Lee JY, Je JH, Ryu WS, Kim HS. A study of the properties of pyrolytic carbons deposited from propane in a tumbling and stationary bed between 900 and 1230°C. *Carbon* 1984;21(6):523–33.
- [8] Li BQ. Gas-particle flows and heat/mass transfer in chemical deposition processes for biomedical applications. In: 1996-99-ENH-PLEX-02 Year 2 Progress Report, Pullman WA: LEQSF, 1996.